applied sciences

MDPI

Article

A Cement Bond Quality Prediction Method Based on a Wide and Deep Neural Network Incorporating Embedded Domain Knowledge

Rengguang Liu [1], Jiawei Yu [2], Luo Liu [1], Zheng Wang [2,3], Shiming Zhou [1] and Zhaopeng Zhu [4,*]

[1] Key Laboratory of Cementing and Completion, Sinope, SINOPEC Research Institute of Petroleum Engineering Co., Ltd., Beijing 102206, China
[2] College of Petroleum Engineering, China University of Petroleum, Beijing 102249, China
[3] Department of Civil and Environmental Engineering, University of Alberta, Edmonton, AB T6G 2C6, Canada
[4] College of Mechanical and Transportation Engineering, China University of Petroleum, Beijing 102249, China
* Correspondence: zhuzp@cup.edu.cn

Abstract: Cement bond quality is critical to ensuring the long-term safety and structural integrity of oil and gas wells. However, due to the complex interdependencies among geological conditions, operational parameters, and fluid properties, accurately predicting cement bond quality remains a considerable challenge. To improve the accuracy and practical applicability of cement bond prediction, this study develops an intelligent prediction model. A Wide and Deep neural network architecture is adopted, into which two key parameters of the cement slurry's power-law rheological model—the consistency coefficient and the flow behavior index—are embedded. A temperature correction mechanism is incorporated by integrating the correction equations directly into the network structure, allowing for a more realistic representation of the cement slurry's behavior under downhole conditions. The proposed model is designed to simultaneously predict the bonding quality at both the casing–cement sheath and cement sheath–formation interfaces. It is trained on a field dataset comprising 30,000 samples from eight wells in an oilfield in western China. On the test set, the model achieved prediction accuracies of 87.29% and 87.49% at the two interfaces, respectively. Furthermore, field testing conducted during a third-stage cementing operation of a well demonstrated a prediction accuracy of approximately 90%, indicating strong adaptability to real-world engineering conditions. The results demonstrate that the temperature-corrected neural network effectively captures the flow characteristics of the cement slurry. The proposed model meets engineering application requirements and serves as a reliable, data-driven tool for optimizing cementing operations and enhancing well integrity.

Keywords: artificial intelligence; cement bond quality prediction; neural network; knowledge embedding

check for updates

Academic Editor: Jose María Alvarez Rodríguez

Received: 13 March 2025
Revised: 21 April 2025
Accepted: 28 April 2025
Published: 14 May 2025

Citation: Liu, R.; Yu, J.; Liu, L.; Wang, Z.; Zhou, S.; Zhu, Z. A Cement Bond Quality Prediction Method Based on a Wide and Deep Neural Network Incorporating Embedded Domain Knowledge. *Appl. Sci.* **2025**, *15*, 5493. https://doi.org/10.3390/app15105493

Copyright: © 2025 by the authors. Licensee MDPI, Basel, Switzerland. This article is an open access article distributed under the terms and conditions of the Creative Commons Attribution (CC BY) license (https://creativecommons.org/licenses/by/4.0/).

1. Introduction

Cementing is a critical stage in oil and gas well construction and plays a key role in ensuring the well's production lifespan [1]. Improving cementing quality has long been a major focus of research in this field. The ability to predict cementing quality before the operation would enable the early identification of high-risk areas and the implementation of effective measures, ultimately enhancing overall cementing performance. However, cementing quality is influenced by numerous interrelated factors, including formation

conditions, wellbore status, fluid properties, and cementing operation parameters [2–4]. The complex interactions among these factors make it challenging to develop a mechanistic model capable of accurately predicting cementing quality. As a result, there is an urgent need for intelligent models capable of capturing nonlinear interactions among multi-source parameters and enabling accurate prejob cement bond quality forecasting.

To address this challenge, scholars have applied various methods to analyze the correlations among key influencing factors. As a result, several preliminary cement bond quality prediction methods have been developed, laying the foundation for further advancements in this field. Li et al. [5] integrated various logging evaluation methods to develop a comprehensive cement bond quality assessment system tailored to different requirements. Kinoshita et al. [6] explored the feasibility of using real-time acoustic measurements for quantitative cement bond quality evaluation. Meanwhile, Sun et al. [7] applied fuzzy evaluation and gray correlation theory to establish a multi-factor statistical method for assessing cement bond quality. Ai et al. [8] developed a multi-factor prediction model for cement bond quality based on an orthogonal scale wavelet network, significantly enhancing computational speed. Sun [9] applied fuzzy evaluation methods and the analytic hierarchy process (AHP) from fuzzy mathematics to establish a multi-factor prediction approach for cement bond quality, enabling the optimization of cementing parameters. The above methods possess a certain degree of scientific validity; however, they lack adaptability to complex and dynamic conditions, and their scalability and generalization capabilities are limited.

In recent years, with the rapid development of artificial intelligence (AI), cement bond quality prediction has witnessed a growing adoption of intelligent methods. A wide range of machine learning models have been explored to enhance prediction accuracy and adaptability under complex downhole conditions. Kong [10] integrated the gray system method with a fuzzy neural network to develop a combined gray–fuzzy neural network approach for cement bond quality prediction, enhancing the model's generalization capability. Guan [11] proposed a cement bond quality prediction method using a least squares support vector machine (LS-SVM), which improved prediction accuracy. Du et al. [12] optimized the BP neural network model using the LM (Levenberg–Marquardt) optimization algorithm, significantly improving the accuracy of cement bond quality prediction. Zhao [13] explored the application of machine learning methods in cement bond quality prediction and introduced the fundamental principles of machine learning models for quality assessment. He et al. [14] analyzed the influencing factors throughout the entire cementing process and applied a gray–fuzzy neural network for prediction, providing data support for cementing operations in deep and ultra-deep wells.

With the increasing availability of high-resolution data, advanced techniques have been proposed to further improve predictive capabilities. Edwin et al. [15] applied gradient boosting regression trees (GBRT) to estimate shear bond strength (SBS) and compressive strength (CS) of fly ash-modified cement, demonstrating superior performance. Fang et al. [16] proposed a multi-scale perceptual CNN that adaptively fuses variable density logging (VDL) features, achieving over 90% accuracy in bond quality identification. Zhang et al. [17] proposed RheologyNet, a physics-informed neural network (PINN) framework that embeds rheological PDEs to capture macro–micro thixotropic behaviors. Amirhossein et al. [18] proposed a transfer learning strategy for cement isolation classification by converting VDL data into continuous wavelet transform (CWT) images and fine-tuning pretrained deep models, achieving accuracies of 97.4% to 99.6%.

These studies demonstrate that artificial intelligence (AI)-based methods offer significant advantages in prediction performance compared with traditional approaches for cement bond quality evaluation. However, existing models still face several critical chal-

lenges in practical applications. First, most current studies primarily rely on well-logging data, often neglecting crucial cementing operational parameters such as displacement efficiency, flow rates, and fluid properties, all of which play a decisive role in the formation of cement bond quality. Some studies utilize CBL-VDL data, which are acquired after the cementing operation. While these data are useful for post-job evaluation, they lack timeliness and are insufficient for proactive optimization or real-time control during the cementing process. Second, certain studies focus on predicting cement sheath characteristics under laboratory conditions without validating the models in complex field environments. This raises concerns about the adaptability and accuracy of such models in real-world applications. Third, most existing research assesses cement bond quality at a holistic level, without distinguishing between the casing–cement sheath interface and the cement sheath–formation interface. However, these two interfaces differ fundamentally in terms of mechanical behavior and failure mechanisms. The absence of interface-level modeling limits the interpretability of the results and reduces their engineering relevance. Therefore, developing high-precision models that integrate multi-source parameters, enable interface-specific prediction, and are adaptable to complex field conditions has become an urgent demand in this field.

To address the aforementioned challenges, this study proposes a novel Wide and Deep neural network architecture capable of simultaneously predicting the cement bond quality at both the casing–cement sheath and cement sheath–formation interfaces. The model is trained and validated on a field dataset comprising 30,000 samples from eight wells in an oilfield located in western China. The consistency coefficient and flow behavior index are embedded into the network structure, and a temperature correction mechanism is incorporated to further enhance prediction accuracy. The objective of this study is to improve the adaptability, interpretability, and accuracy of cement bond quality prediction models, thereby providing reliable data-driven support for optimizing cementing design and reducing operational risks.

2. Methodology

The objective of this study is to develop a physically informed neural network model capable of accurately predicting cement bond quality at both the casing–cement sheath and cement sheath–formation interfaces. To achieve this, a multi-stage workflow was designed, as illustrated in Figure 1.

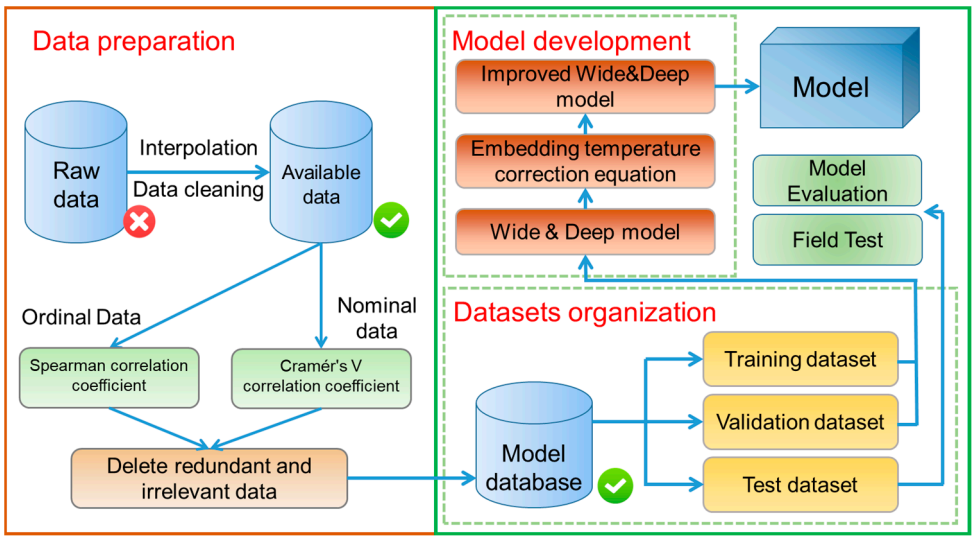


Figure 1. Workflow of this study.

First, raw field data were subjected to initial screening, followed by interpolation and preprocessing to improve data completeness and reliability. To ensure the relevance of input features, correlation analysis was performed using Spearman's Rank Correlation Coefficient (for continuous variables) and Cramér's V (for categorical variables). Variables with low correlation to cement bond quality were excluded to avoid noise and overfitting. The cleaned and filtered dataset was then split into training, validation, and testing subsets, ensuring no overlap to maintain model generalization.

During the construction of the neural network model, the key influencing factors were categorized into cementing operation data and geological engineering data. According to relevant literature [19–21] and the experience of field engineers, cementing operational parameters (such as cement slurry density, viscosity, preflush density, and slurry flow rate) largely determine the cement bond quality, while formation and engineering characteristics (such as well depth, well inclination, wellbore temperature, and annular clearance) reflect the complexity of the cementing environment and indirectly affect the bond quality by influencing operational and environmental conditions during the cementing process. Based on these interrelationships, this study developed a Wide and Deep neural network model, integrating shallow and deep features to improve prediction accuracy.

Considering the significant impact of cement slurry rheology on bonding performance—and its temperature sensitivity—the study incorporated a power-law rheological model. Rheological parameters were calculated using data from five-speed rotational viscometers and corrected for temperature variations through nonlinear fitting. The corrected rheological values were then embedded into the neural network input structure as domain-specific features, enhancing the physical interpretability and generalization capability of the model.

Finally, the model was trained and tested on over 30,000 records collected from eight wells in an oilfield located in western China, followed by field testing. Through multiple iterations of training and evaluation, a high-performance cement bond quality prediction model was established, providing practical support for prejob cementing risk control and parameter optimization.

2.1. Data Organization

The dataset used in this study was obtained from cemented wells in a certain oilfield in western China. An in-depth analysis and effective utilization of geological and engineering information are crucial for enhancing cement bond quality, improving operational efficiency, and driving the continuous advancement of cementing technology. Geological conditions directly influence the selection of cementing materials and their sealing performance, while drilling operation quality indirectly affects the actual execution of cementing [22]. Additionally, cementing techniques and processes ultimately determine the overall cementing effectiveness.

This study identified the key factors affecting cement bond quality across three critical dimensions: geological characteristics, drilling operations, and cementing processes. To enable a comprehensive analysis, a database was developed, integrating three major categories of parameters—geological, drilling, and cementing—comprising over 30,000 sample entries. A detailed summary of the identified influencing factors is presented in Table 1.

2.2. Data Preprocessing

Data preprocessing plays a vital role in data analysis and model development. Raw data often contain missing values, outliers, and various inconsistencies which, if not properly addressed, can significantly degrade model performance and prediction accuracy. In this study, the original well-logging dataset contained both outliers and missing

values. To ensure data quality and integrity, a comprehensive preprocessing pipeline was implemented.

Table 1. Factors affecting cement bond quality and their classification.

Category	Feature	Variable	Category	Feature	Variable
Drilling	Well depth	x_1	Cementing	Casing size	x_{11}
	Borehole diameter	x_2		Centralizer position	x_{12}
	Drill bit size	x_3		Drilling fluid density	x_{13}
	Deviation angle	x_4		Preflush density	x_{14}
	Azimuth angle	x_5		Cement slurry density	x_{15}
Geological	Formation fluid density	x_6		Cement slurry flow rate	x_{16}
	Acoustic travel time	x_7		Preflush flow rate	x_{17}
	Wellbore temperature	x_8		Rheological Properties	x_{18}
	Gamma ray	x_9		Annular clearance	x_{19}
	Wellbore pressure	x_{10}		Water-cement ratio	x_{20}

First, outlier detection was performed using the K-means clustering algorithm. K-means effectively groups similar data points into clusters, while abnormal data points tend to fall on the periphery of clusters or form small, isolated groups—making them easier to identify. During clustering, the data were partitioned into K clusters, and potential outliers were identified based on their distance from the cluster centroids. If a data point's distance exceeded the predefined cluster radius, it was flagged as an outlier. The absolute distance was calculated using the following method:

$$\mathrm{d}\left(\vec{x}_i, \vec{x}_j\right) = \sum_{k=1}^{p} \left| x_{ik} - x_{jk} \right| \tag{1}$$

where $\vec{x}_i = \left(x_{i1}, x_{i2}, \ldots, x_{ip}\right)'$, $\vec{x}_j = \left(x_{j1}, x_{j2}, \ldots, x_{jp}\right)'$, $\vec{x}$ is a feature vector.

For missing values, appropriate interpolation methods were applied based on the nature of each variable. These methods ensured data completeness and preserved the statistical characteristics of the dataset, thereby improving the robustness of the model during training.

To predict cement bond quality, a 1 m interval was chosen as the minimum unit for analysis. All input data for the models were interpolated at 1 m intervals and aligned along the depth domain to ensure consistency and accuracy in the model inputs. The azimuthal angle, being cyclical (ranging from 0° to 360° or equivalently in radians), poses challenges for linear interpolation, as it may introduce discontinuities (e.g., interpolating between 350° and 10° incorrectly spans the full range). A cylindrical helix interpolation method was used to address this issue, ensuring smooth and consistent interpolated values. Other data were processed using the linear interpolation method.

Casing centralizers were not installed on every casing section. For this study, the positions where centralizers were installed were encoded as "1", while positions without centralizers were encoded as "0".

The supervised learning model developed in this study predicts the cement bond quality of both the interface between the casing and the cement sheath, and the interface between the cement sheath and the formation. Based on the interpretation results of acoustic amplitude and variable-density logging results, the quality of these two interfaces

can be classified into three categories: good, moderate, and poor. We also used these three indices to label the cement bond quality in this study.

2.3. Feature Selection

Feature selection is a crucial step in machine learning and data analysis, aiming to identify the most influential features while eliminating redundant ones to enhance model efficiency and accuracy. To achieve this, we conducted a correlation analysis to remove variables with minimal impact.

Spearman's rank correlation coefficient is a nonparametric statistical method used to measure the monotonic relationship between two variables [23]. It is particularly suitable for data that are nonnormally distributed, contain outliers, or exhibit nonlinear correlations. The calculation formula is as follows:

$$\rho = 1 - \frac{6\sum d_i^2}{n(n^2-1)} \tag{2}$$

where $d_i = R(X_i) - R(Y_i)$, which represents the rank difference between the two variables for each observation. $R(X_i)$ and $R(Y_i)$, respectively, represent the ranks of variable X_i and variable Y_i.

n is the number of data samples.

The value of ρ ranges from -1 to 1. $\rho = 1$: perfect positive correlation, meaning that as one variable increases, the other also increases. $\rho = -1$: perfect negative correlation, meaning that as one variable increases, the other decreases. $\rho = 0$: no correlation, indicating no monotonic relationship between the variables.

The Spearman correlation coefficient matrices between various influencing factors and the casing–cement interface and cement–formation interface are shown in Figures 2a and 2b, respectively.

In the Spearman correlation coefficient matrix heatmap, different colors represent the strength of the correlation between variables: Red (close to 1.0, strong positive correlation): Indicates a strong positive relationship between variables, meaning that as one variable increases, the other also tends to increase. Blue (close to -1.0, strong negative correlation): Indicates a strong negative relationship, meaning that as one variable increases, the other tends to decrease. Near-white or light-colored areas (close to 0.0): Suggest little to no correlation between the variables. Among these variables, x1 to x19 correspond to those listed in Table 1, while y1 and y2 represent the casing–cement interface and cement–formation interface quality, respectively.

x1 (well depth) and x8 (wellbore temperature) show a strong correlation ($\rho = 0.97$), indicating that they provide highly redundant information. To reduce redundancy, this study discards wellbore temperature (x8), as it is less essential. x6 and x10 exhibit a strong negative correlation ($\rho = -0.97$), suggesting that one of them should be removed to optimize variable selection. This study chooses to discard Wellbore Pressure (x10) for better feature selection.

Strongly correlated influencing factors include x16 (cement slurry flow rate) and x17 (preflush flow rate), with correlation coefficients of -0.71 and 0.61, respectively. These variables should be given special attention during the cementing process to optimize cementing quality. The correlation coefficient between x5 (Azimuth) and the casing–cement interface quality is low (-0.07). Therefore, it is not considered in the analysis. A similar trend is observed in Figure 2b, indicating that different variables also exhibit comparable effects on the cement–formation interface quality (y2).

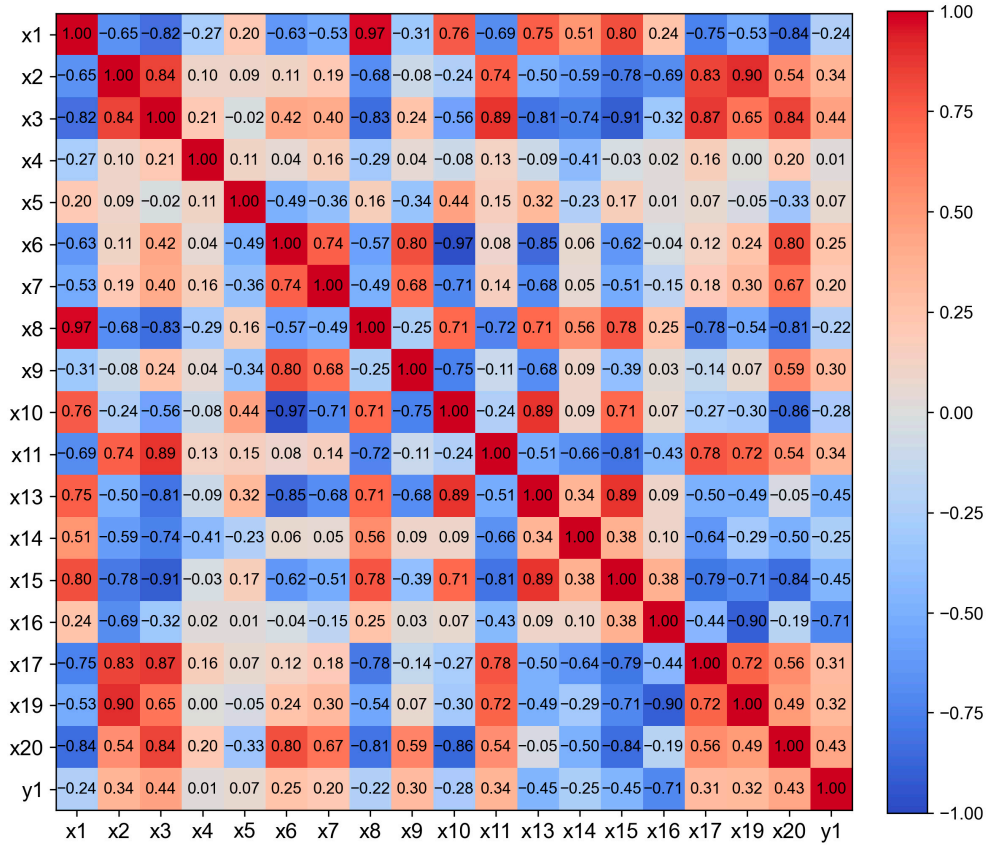


Figure 2. Spearman correlation coefficient matrix: (**a**) Casing-cement sheath interface; (**b**) Cement sheath-formation interface.

Since the centralizer position data are discontinuous and represented as a binary sequence (0 and 1), it is not suitable for direct calculation using the Spearman correlation coefficient. Instead, Cramér's V correlation coefficient is used for analyzing the correlation coefficients among discrete variables [24]. The Cramér's V coefficient also lies within the range of 0 to 1. $V = 0$ indicates no association between two categorical variables. $V = 1$, indicates a perfect association. It is calculated as follows:

$$V = \sqrt{\frac{\chi^2}{n \cdot min(k-1, r-1)}} \tag{3}$$

where the following are used:

χ^2: the chi-square statistic.

n: the total number of observations.

k: the number of categories in the column variable.

r: the number of categories in the row variable.

$min(k-1, r-1)$: the smaller of the degrees of freedom for rows or columns.

The correlation coefficients between the centralizer position and the cement bond quality at the two interfaces were calculated using Equation (3). The calculation results are shown in Figure 3. From the figure, it is evident that the casing–cement interface quality and cement–formation interface quality are influenced by the centralizer position. Therefore, it should be taken into consideration in the analysis.

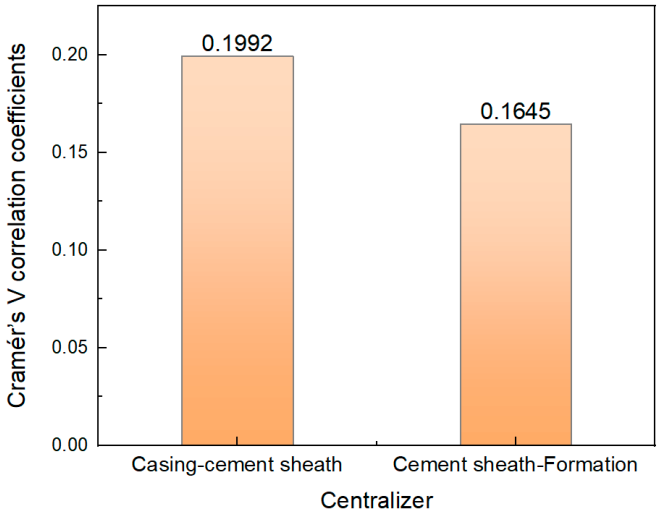


Figure 3. Cramér's V correlation coefficients between centralizer position and the cement bond quality of both interfaces.

2.4. Data Normalization

Data normalization is a commonly used data preprocessing technique aimed at handling data with different scales and units. This process normalizes the data to a uniform range and reduces the impact of differences in magnitude, features, and distributions on the model. Common normalization methods include Z-Score and Min-Max normalization.

Considering that the data used in this study vary with depth, and variables such as well depth and deviation angle do not follow a normal distribution, Min-Max normalization was chosen as the data normalization method. This method linearly transforms the original data to constrain it within the range of [1], eliminating dimensional differences and mitigating the impact of varying magnitudes of parameters on model performance. The transformation is defined as follows:

$$x* = \frac{x - x_{min}}{x_{max} - x_{min}} \tag{4}$$

where the following are used:

x represents the original data.

x_{min} and x_{max} are the minimum and maximum values of the data, respectively.

$x*$ is the normalized data.

3. Model Development and Evaluation

3.1. Principles of Neural Networks

The fundamental unit of a neural network is the neuron. In 1943, McCulloch and Pitts, inspired by the biological nervous system, abstracted it into a simple mathematical model [25], as shown in Figure 4.

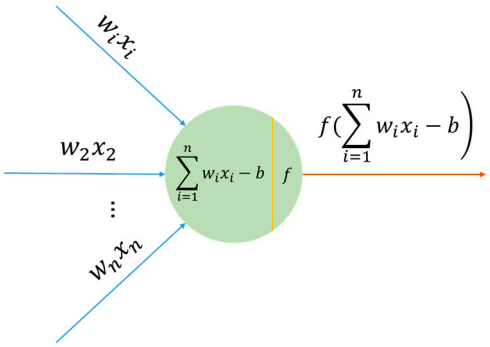


Figure 4. Neuron schematic diagram.

A neuron receives input signals x_i from other neurons, which are weighted by w_i. The total input is then computed and compared with a threshold b. The final output of the neuron is generated by applying an activation function f to the processed input. The forward propagation process is expressed as follows:

$$y = f\left(\sum_{i=1}^{n} w_i x_i - b\right) \tag{5}$$

3.2. Model Development

The Wide and Deep neural network model is an integrated machine learning framework first proposed by Google [26]. The core idea of this model is to combine a wide model (wide) with a deep neural network (deep) to simultaneously capture both linear and nonlinear relationships among features.

The neural network structure consists of two components: The wide part and the deep part. The wide part is a linear model, typically used for inputting explicit features. The deep part, on the other hand, is a deep neural network that excels at capturing complex and high-order nonlinear relationships between features.

In the context of cement bond quality prediction, key fluid parameters such as the density of the preflush, spacer fluid, and cement slurry, as well as operational parameters including displacement rate, and centralizer position, directly influence the final cement bond quality. Therefore, in the neural network architecture design, these parameters are input into the wide component and directly connected to the output layer to enhance the model's analytical capability for direct influencing factors. Meanwhile, formation characteristics such as well depth, deviation angle, which interact and are interdependent, are input into the deep component to effectively capture their complex nonlinear relationships, thereby reflecting the difficulty of the current cementing environment. The wide and deep components interact synergistically to optimize the model's predictive performance and

ultimately output the cement bond quality. The overall structure of the neural network model is illustrated in Figure 5.

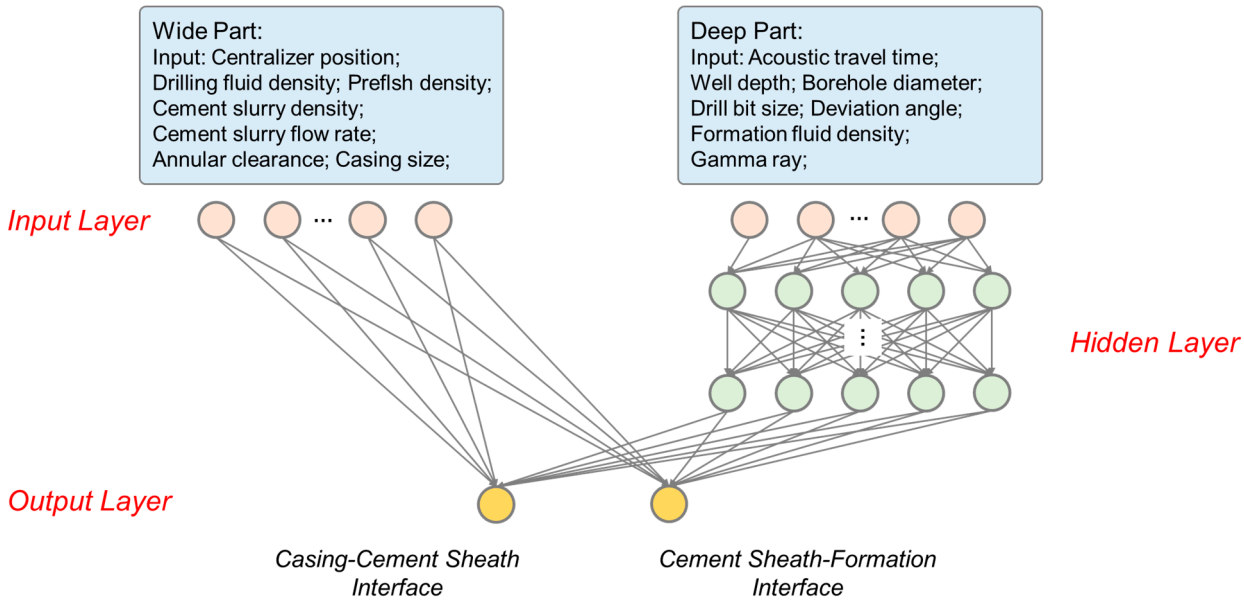


Figure 5. Wide and Deep neural network architecture.

3.3. Model Evaluation Method

The primary metrics used for evaluating the classification performance of the model include classification accuracy (also known as precision), recall, and precision. In this paper, these three metrics are mainly used to assess the performance of the proposed method. Figure 6 shows the confusion matrix showing the four elements: true positive (TP), false negative (FN), false positive (FP), and true negative (TN).

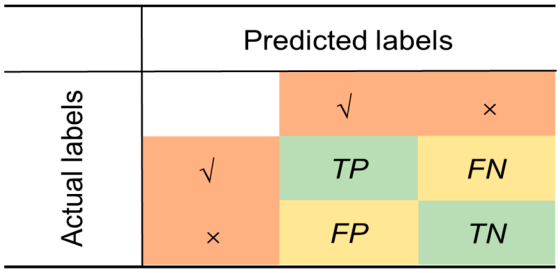


Figure 6. Confusion matrix.

Accordingly, we can use the following equations to calculate the classification accuracy (ACC), recall (R), precision (P), and F1-score:

$$ACC = \frac{TP + TN}{TP + FP + TN + FN} \tag{6}$$

$$R = \frac{TP}{TP + FN} \tag{7}$$

$$P = \frac{TP}{TP + FP} \tag{8}$$

$$\mathrm{F1} = \frac{2PR}{P + R} \tag{9}$$

4. Result

All the numerical experiments were conducted using the following computer configurations: A Windows 11 operating system, an Intel Xeon E5 processor, a 128 GB RAM, and an NVIDIA RTX2060 Super GPU with 12 GB video memory. The deep neural network model was implemented using the Python 3.7 programming language and the PyTorch 1.10 (GPU version) deep learning framework.

4.1. Wide and Deep Neural Network

The dataset used in this study consists of 30,000 entries from a certain oilfield in western China, which were utilized for model training and validation, with a training-to-testing ratio of 7:3. The test dataset includes 9000 samples, which were used for model testing and were not involved in the training process. The numerical experiment results are summarized in Figure 7.

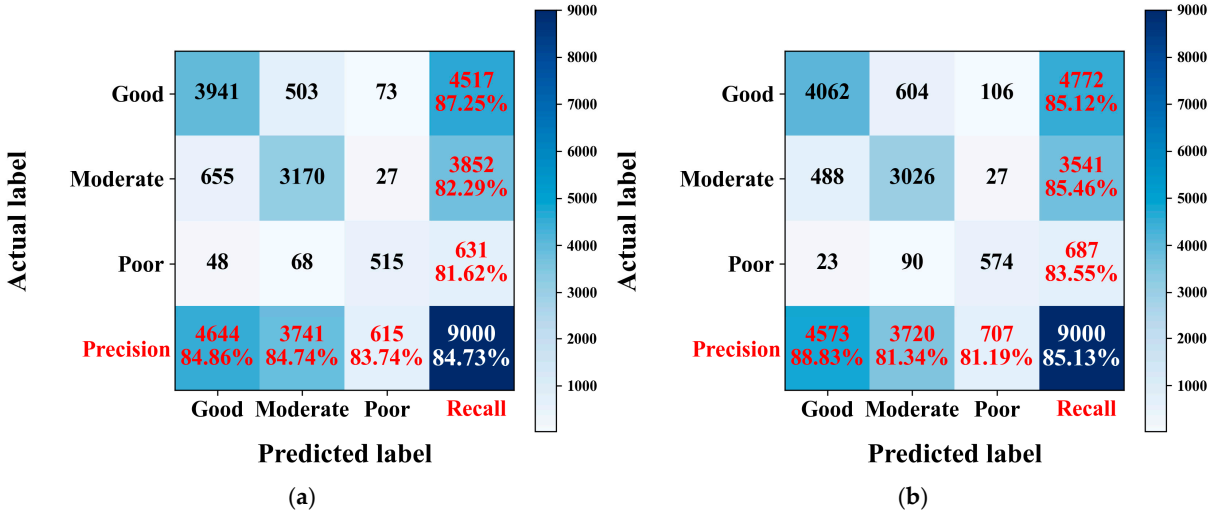


Figure 7. Confusion matrices of the Wide & Deep model predictions: (**a**) cement bond quality at the casing–cement sheath and (**b**) cement bond quality at the cement sheath–formation interface.

Figure 7 shows two confusion matrices. In these confusion matrices, the horizontal axis (Predicted label) represents the labels predicted by the model (Good, Moderate, Poor). The vertical axis (Actual label) represents the actual labels (Good, Moderate, Poor). The numbers in each cell represent the number of matchings between the actual labels and the predicted labels. The color bar in the figure reflects the magnitude of the values in each cell. The numbers along the diagonal represent correctly classified instances. The darker the color of the diagonal cells, the larger the values, indicating higher prediction accuracy, while lighter colors suggest lower accuracy. Based on this figure, we can calculate precision and recall and subsequently derive the F1-score. The calculated results are summarized in Tables 2 and 3 and visualized in Figure 8.

Table 2. Recall, Precision, and F1-score generated for predicting cement bond quality at the casing–cement sheath interface using the Wide & Deep model.

	Good	Moderate	Poor
Recall	87.24%	82.29%	81.62%
Precision	84.86%	84.73%	83.74%
F1-score	0.8603	0.8350	0.8266

Table 3. Recall, Precision, and F1-score generated for predicting cement bond quality at the cement sheath–formation interface using the Wide & Deep model.

	Good	Moderate	Poor
Recall	85.12%	85.46%	83.55%
Precision	88.83%	81.34%	81.19%
F1-score	0.8693	0.8335	0.8235

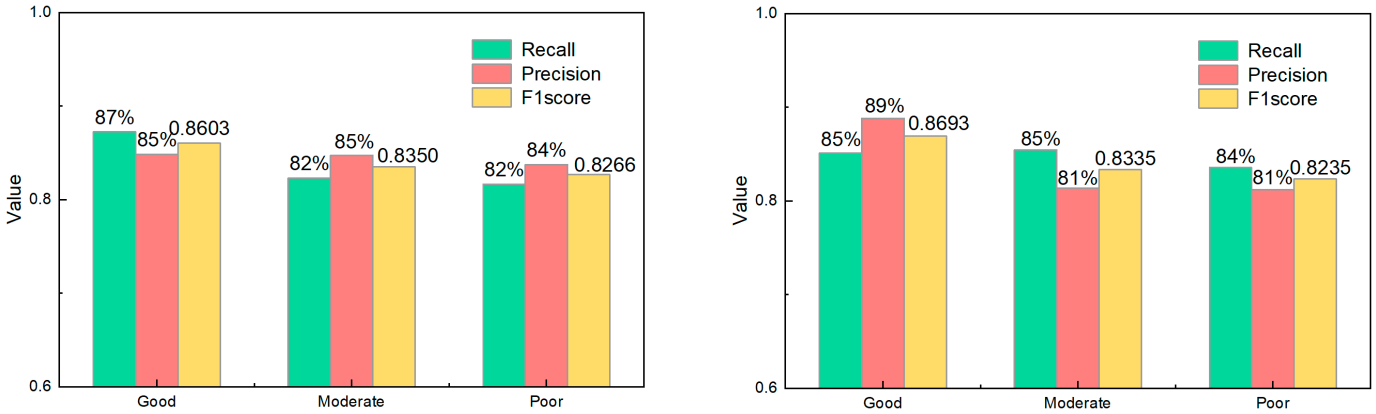


Figure 8. Recall, precision, and F1-score generated (**a**) cement bond quality at the casing–cement sheath and (**b**) cement bond quality at the cement sheath–formation interface, using the Wide & Deep model.

From the results in Figure 8, it can be observed that the Good category exhibits the best recognition performance. In both interfaces—(a) casing–cement sheath and (b) cement sheath–formation—the F1-scores reach 0.8576 and 0.8679, respectively, indicating a high classification accuracy and the model's strong ability to identify this category.

In contrast, the recognition performance for the Moderate and Poor categories is relatively lower, primarily due to a decrease in precision, which consequently leads to a lower F1-score. This may be attributed to significant data overlap or ambiguity between the Moderate and Poor categories, making it challenging for the model to distinguish between them and thereby affecting classification accuracy. Therefore, to enhance overall recognition performance, further optimization of the model structure is required.

4.2. Domain Knowledge Embedding

The research findings in Section 4.1 indicate that while the current model has achieved a certain level of accuracy in predicting cement bond quality, its recognition rate for poor cementing conditions is only around 80%, which is precisely our primary concern. This level of accuracy remains insufficient for practical engineering applications, highlighting the need for further model optimization to enhance its ability to identify poor-cement bond quality, thereby improving engineering reliability and applicability.

The flowability of cement slurry is crucial to the quality of well cementing [27,28]. During the static phase, as the slurry undergoes hydration, changes in shear stress directly influence its thixotropy, suspension stability, and further affect drilling fluid displacement efficiency and final cementing quality [29,30].

If the shear stress is too low, the cement slurry may fail to effectively scour the wellbore, leading to residual mud cake, which in turn degrades the cement bond and reduces cementing quality. Conversely, excessively high shear stress may result in uneven slurry flow, causing poor laminar flow control and ultimately reducing displacement

efficiency. Therefore, an optimal shear stress level is essential, as it promotes the formation of a stable helical flow, enhances annular displacement efficiency, and effectively removes drilling fluid, thereby ensuring superior cement bond quality.

According to research, cement slurry systems generally exhibit Bingham plastic or power-law rheological behavior, as detailed below:

Bingham Plastic Model [31]:

$$\tau = \tau_y + \mu_p \dot{\gamma} \tag{10}$$

where the following are used:

τ: shear stress (Pa);

τ_y: yield stress (Pa);

μ_p: plastic viscosity (Pa·s);

$\dot{\gamma}$: shear rate (s^{-1}).

Power-law Model [32]:

$$\tau = k\dot{\gamma}^n \tag{11}$$

where the following are used:

k: consistency coefficient ($Pa \cdot s^n$);

n: flow behavior index (dimensionless).

This study analyzes the field test results of cement slurry, utilizing a five-speed rotational viscometer to conduct rheological experiments under both ambient and high-temperature conditions. By analyzing the experimental data, the flow pattern of the cement slurry can be determined, enabling a more accurate characterization of its rheological properties. Figure 9 presents the rheological test results of cement slurry used in the second and third casing sections of a well. Based on the experimental data, curve fitting is performed to further quantify the rheological parameters of the cement slurry.

In Figure 9, the blue dashed line represents the Bingham model fitting curve, while the orange dashed line represents the power-law model fitting curve. By comparing Figure 9a,b, the following conclusion can be drawn: At 25 °C, the power-law model achieves a fitting accuracy of R^2 = 1.000, which is higher than that of the Bingham model (R^2 = 0.997), indicating that the power-law model provides better fitting precision at this temperature. At 93 °C, the power-law model still maintains R^2 = 1.000, outperforming the Bingham model in terms of fitting accuracy. By comparing Figure 9c,d, similar conclusions can be drawn, confirming that the power-law model consistently outperforms the Bingham model across different temperature conditions, providing a more accurate description of the rheological properties of cement slurry.

Additionally, the rheological curve fitting results for cement slurry from other wells are presented in Appendix A, further validating this conclusion. Therefore, this study recommends using the power-law model to calculate the rheological properties of cement slurry for a more precise characterization of its flow behavior.

During the actual cementing process, there are significant temperature variations at different depths of the wellbore. If the rheological parameters are not corrected for temperature, it may lead to inaccurate predictions of the cement slurry's flow behavior throughout the wellbore [33,34]. In this study, the power-law equation was modified to account for temperature effects, resulting in the corrected formula shown in Equations (12)–(14). Based on this corrected model, the rheological properties of the second-stage and third-stage cementing slurries for this well were fitted, with the results presented in Figure 10.

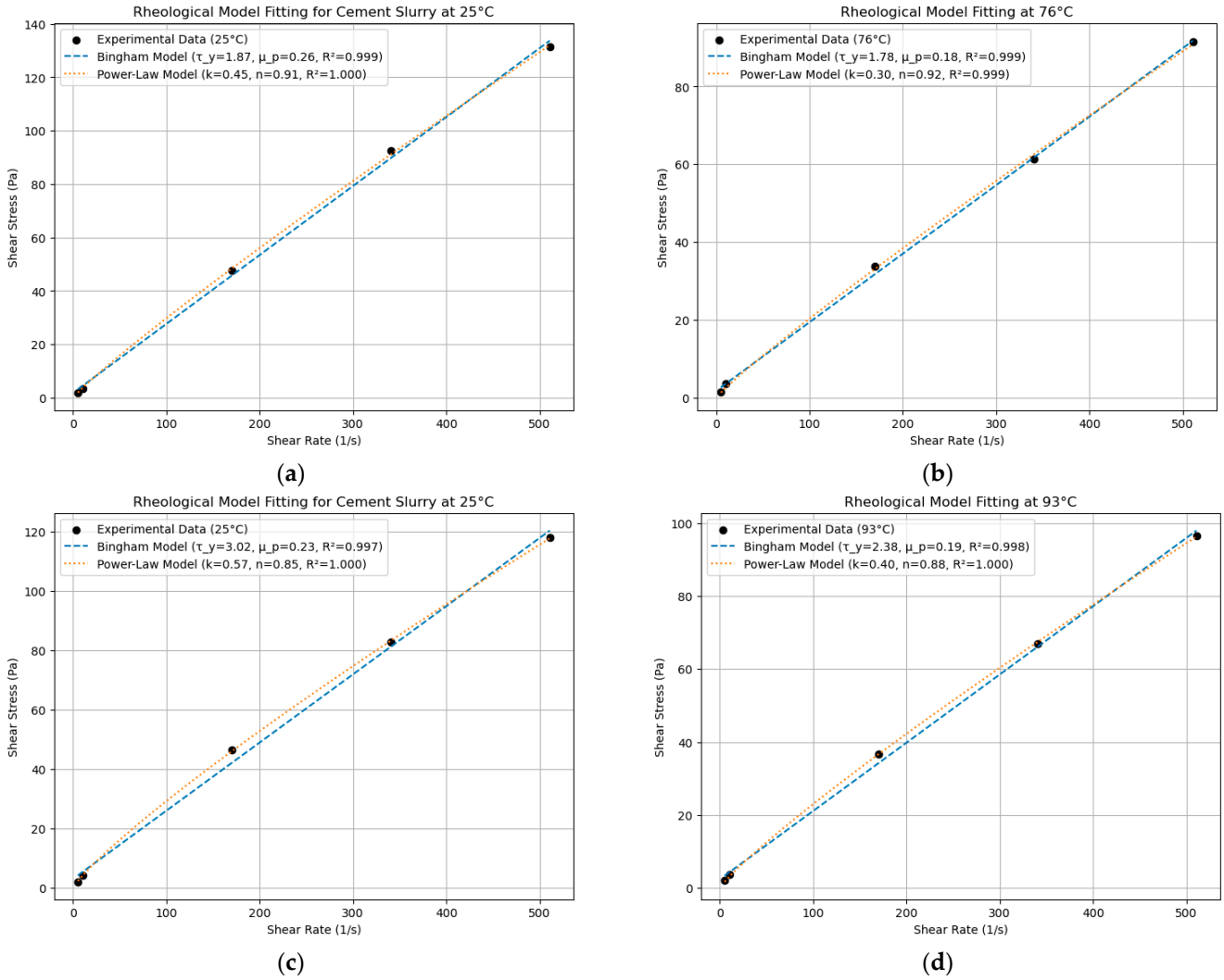


Figure 9. Rheological equation fitting results of cement slurry: (**a**) Second-stage cementing slurry at 25 °C. (**b**) Second-stage cementing slurry at 76 °C. (**c**) Third-stage cementing slurry at 25 °C. (**d**) Third-stage cementing slurry at 93 °C.

$$\tau = k(T)\dot{\gamma}^{n(T)} \tag{12}$$

$$k(T) = k_0 \times e^{-C_k(T-25)} \tag{13}$$

$$n(T) = n_0 \times e^{-C_n(T-25)} \tag{14}$$

where the following are used:

T: temperature (°C);

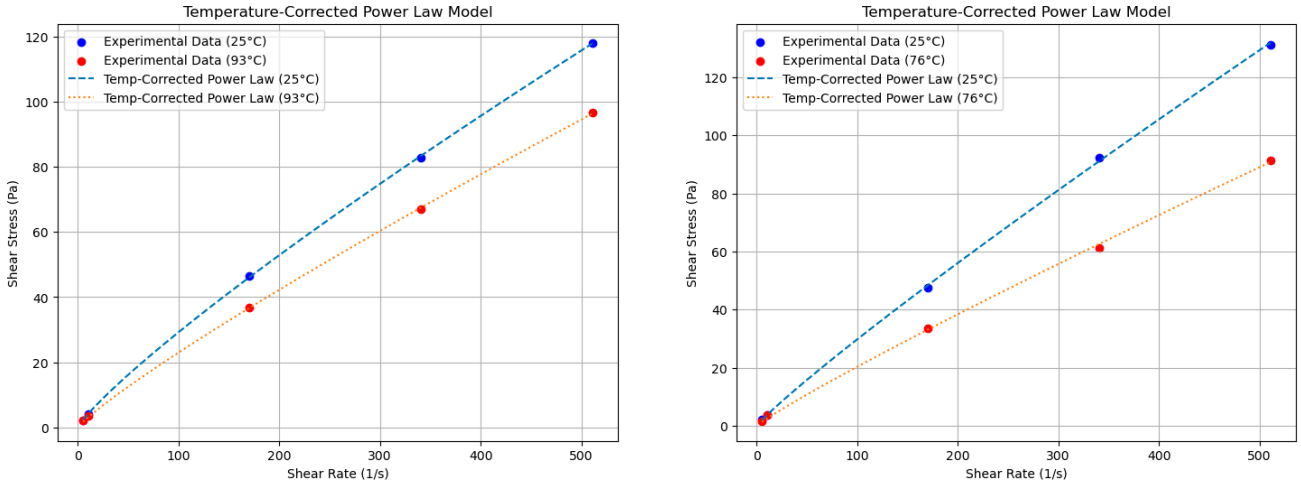
C_k, C_n: temperature influence coefficient;

k_0, n_0: fitted parameter.

In Figure 10a,b, the experimental data (red/blue points) show a high degree of fit with the temperature-corrected power-law model (dashed lines), with R^2 values close to 1. This indicates that the temperature-corrected power-law equation can accurately describe the rheological properties of cement slurry at different temperatures.

In the power-law fluid Equation (12), the consistency coefficient k and the flow behavior index n are key parameters representing the flow characteristics of the fluid. To verify whether temperature correction affects the relationship between cement slurry flow parameters and cementing quality, this study calculated the consistency coefficient and

flow behavior index both with and without temperature correction based on Equation (2) and analyzed their correlation with the interface bond quality between the cement sheath and formation, as well as between the casing and cement sheath. The corresponding results are presented in the form of bar charts, as shown in Figure 11.



$k_0 = 0.570459,\ C_k = 0.005171,\ n_0 = 0.854774,$
$C_n = -0.000408,\ R^2 = 0.999925$
(a)

$k_0 = 0.446754,\ C_k = 0.005979,\ n_0 = 0.912092,$
$C_n = -0.000086,\ R^2 = 0.999658$
(b)

Figure 10. Cement slurry rheology fitting results: (**a**) Third-stage cementing slurry. (**b**) Second-stage cementing slurry.

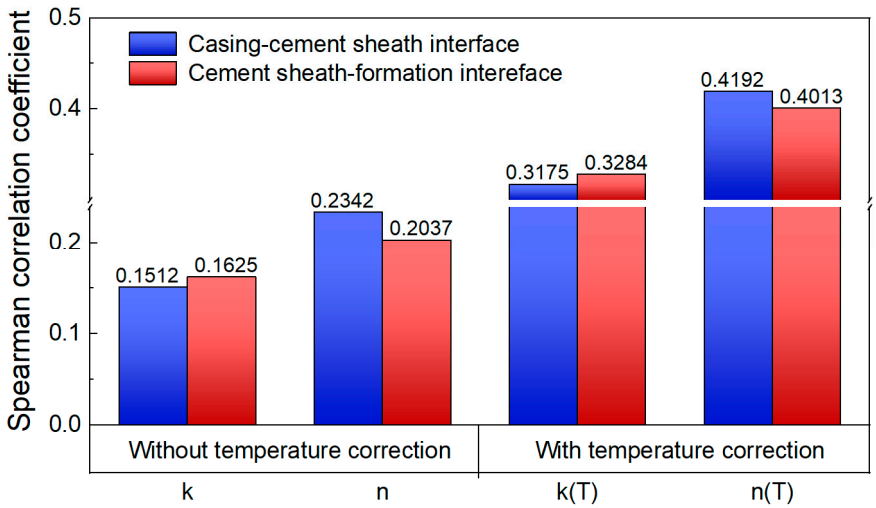


Figure 11. Comparison of Spearman correlation coefficients between rheological parameters and interface bond quality with and without temperature correction.

The uncorrected consistency coefficient k and flow behavior index n exhibit relatively weak correlations with both the casing–cement sheath interface and the cement sheath–formation interface quality, with Spearman correlation coefficients of 0.1512, 0.1625, and 0.2342, 0.2037, respectively. However, after incorporating temperature effects, the corrected parameters $k(T)$ and $n(T)$ show significantly improved correlations, reaching 0.3175, 0.3284, and 0.4192, 0.4013, respectively. This enhancement indicates that the temperature-corrected consistency coefficient and flow behavior index more accurately reflect the actual rheological behavior of the cement slurry under downhole conditions. Therefore, to achieve more reliable predictions of cement bond quality, it is recommended to adopt temperature-corrected rheological parameters as input indicators.

Therefore, we redesigned the neural network model, as illustrated in Figure 12. In this new architecture, a module named "Flowability Characterization Neurons" was introduced. This module incorporates the temperature-corrected consistency coefficient and flow behavior index as independent neurons, which are embedded into the model structure and directly influence the output layer. This enhancement significantly improves the model's ability to represent the actual downhole rheological behavior of cement slurry.

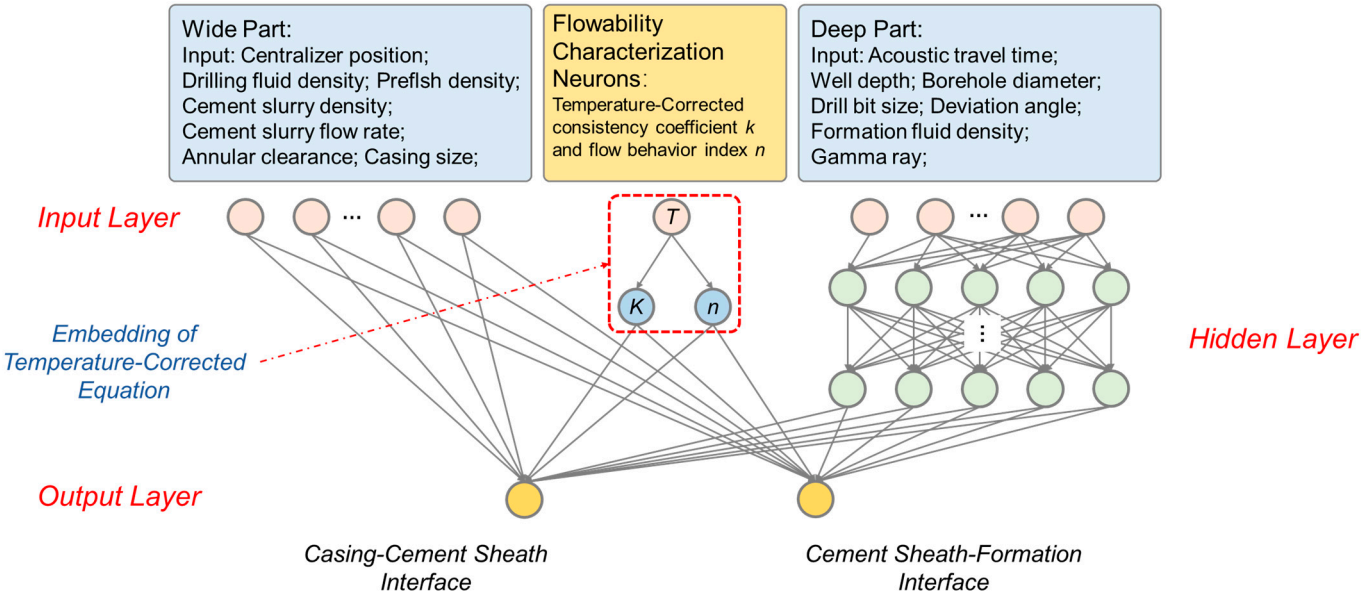


Figure 12. Improved wide and deep neural network architecture.

Conventional neural networks typically adopt the linear transformation form wx+b as the fundamental structure of neurons. In this study, a physics-informed embedding approach is proposed, wherein the traditional linear mapping is replaced by temperature-corrected rheological equations, as defined in Equations (13) and (14). During backpropagation, the nodes governed by these physical equations are automatically differentiated using the chain rule, and their corresponding gradient expressions are given as follows:

$$\frac{\partial k(T)}{\partial T} = -C_k \cdot k(T) \tag{15}$$

$$\frac{\partial n(T)}{\partial T} = -C_n \cdot n(T) \tag{16}$$

To evaluate the impact of embedding temperature-corrected rheological equations into neural networks, a comparative experiment was designed with two structurally consistent models:

Model A adopts the proposed Wide and Deep (WD) architecture, as illustrated in Figure 12. The relationship between downhole temperature and the rheological parameters—consistency coefficient k and flow behavior index n—is explicitly defined by Equations (13) and (14), and these temperature-corrected values are embedded as intermediate neurons into the network.

Model B shares the same overall structure and input features, including temperature. However, instead of using physically derived equations, the intermediate neurons k and n are generated via simple learnable linear transformations of temperature, i.e., y = wx + b.

Both models were trained for 200 epochs, during which the average gradients of the k and n neurons with respect to the downstream fully connected layer were recorded.

This gradient-based analysis enables a direct comparison of model sensitivity and feature utilization under the two embedding strategies. The results are presented in Figure 13.

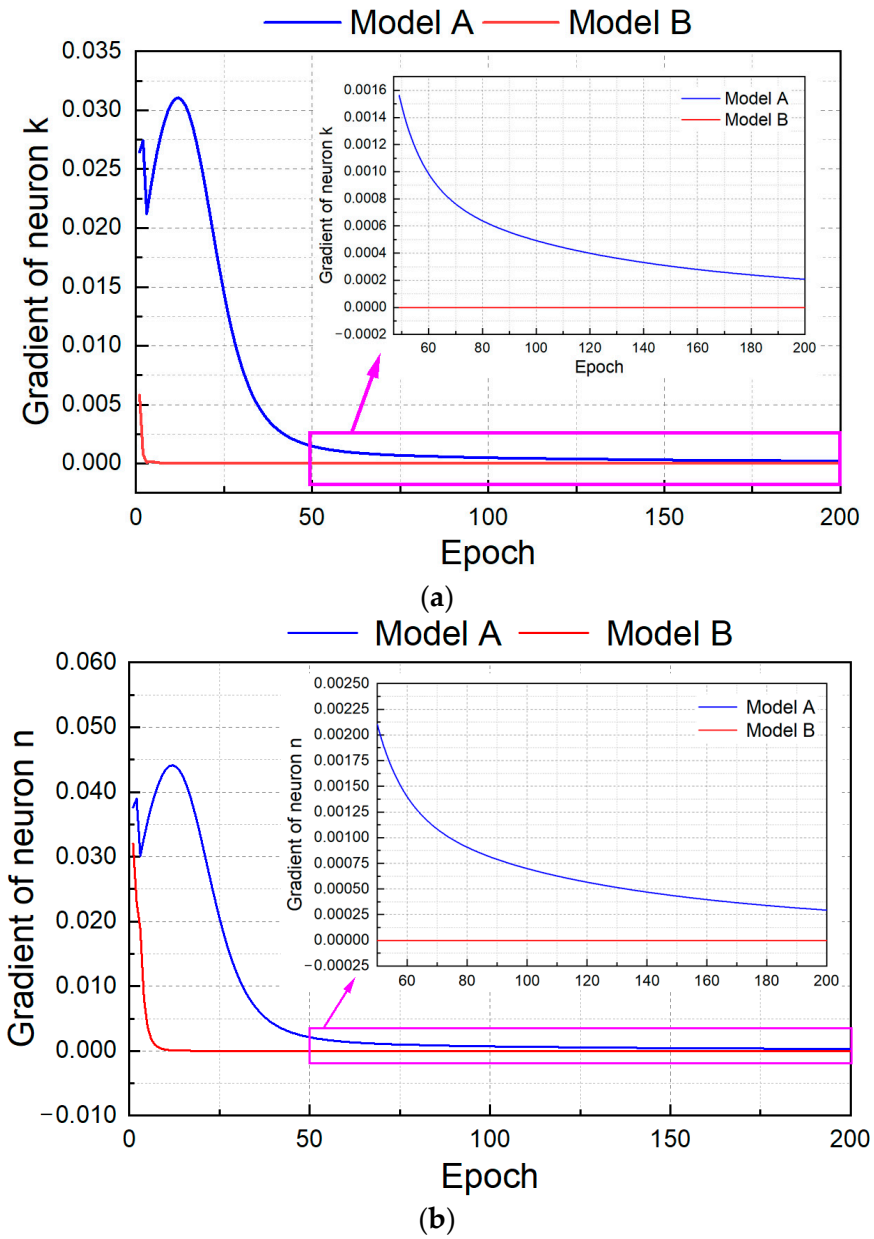


Figure 13. Gradient of neurons during model training: (**a**) Neuron k. (**b**) Neuron n.

As shown in the figure, the average gradients of the k and n neurons in Model A remain consistently high throughout the training process, indicating that the model continuously attends to these physical features—the consistency coefficient k and the flow behavior index n. In contrast, in Model B, where k and n neurons are generated through simple linear mappings (designed to maintain structural consistency but lacking physical significance), their gradients rapidly decay to near zero within the first 50 epochs. This suggests that the Model B fails to effectively utilize these features. These results demonstrate that embedding physical equations enhances the model's sensitivity to critical variables, thereby improving both learning efficiency and interpretability.

4.3. Model Comparison

To evaluate the effectiveness of the improved Wide and Deep model, this study uses the same training and test datasets as those in Section 4.1 for testing. The numerical experiment results are summarized in Figure 14. Based on this figure, we can calculate precision and recall and subsequently derive the F1-score. The calculated results are summarized in Tables 4 and 5 and visualized in Figure 15.

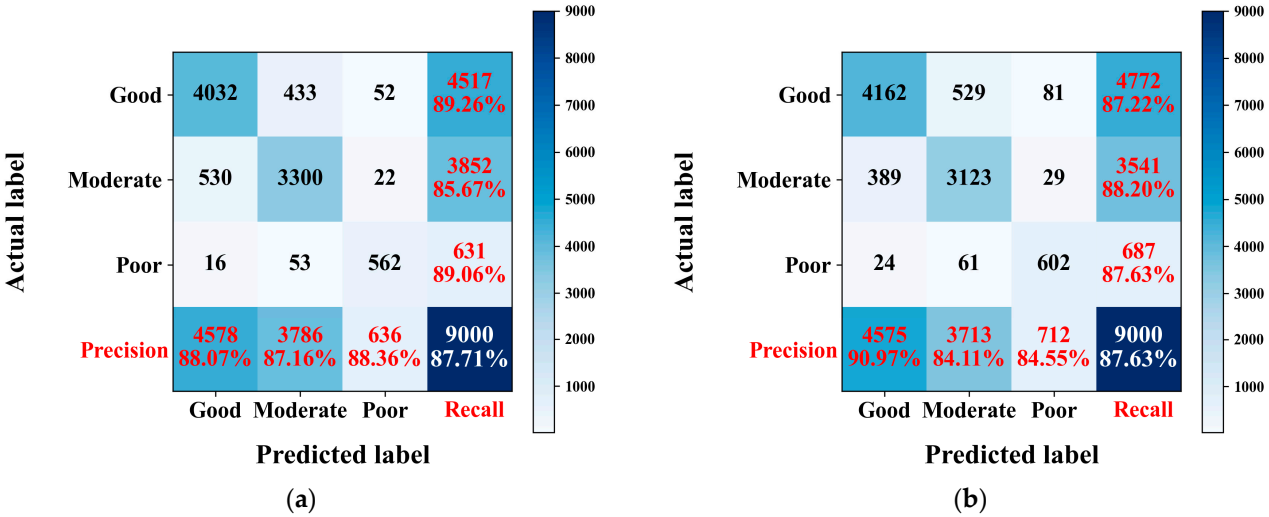


Figure 14. Confusion matrices of the Wide & Deep model embedded with domain knowledge for predicting: (**a**) cement bond quality at the casing–cement sheath and (**b**) cement bond quality at the cement sheath–formation interface.

Table 4. Recall, Precision, and F1-score generated for predicting cement bond quality at the casing–cement sheath interface, using the Wide & Deep model incorporating embedded domain knowledge.

	Good	Moderate	Poor
Recall	89.26%	85.67%	89.01%
Precision	88.07%	87.16%	88.36%
F1-score	0.8866	0.8641	0.8869

Table 5. Recall, Precision, and F1-score generated for predicting cement bond quality at the cement sheath–formation interface, using the Wide & Deep model incorporating embedded domain knowledge.

	Good	Moderate	Poor
Recall	87.22%	88.20%	87.62%
Precision	90.97%	84.11%	84.55%
F1-score	0.8906	0.8611	0.8606

To provide a more intuitive comparison of the model's performance before and after improvement, we present Figure 16. As shown in the figure, the improved model demonstrates better performance across all categories (Good, Moderate, Poor), with higher recall (blue), precision (red), and F1-score (green) compared with the previous model (dashed lines). The F1-score shows a significant increase, indicating a better balance between precision and recall in the optimized model. The recall improvement is the most pronounced, particularly in the 'Poor' category, suggesting that the enhanced model has a stronger capability in identifying more challenging classification cases.



Figure 15. Recall, precision, and F1-score generated for: (**a**) cement bond quality at the casing–cement sheath interface and (**b**) cement bond quality at the cement sheath–formation interface, using the Wide & Deep model incorporating embedded domain knowledge.

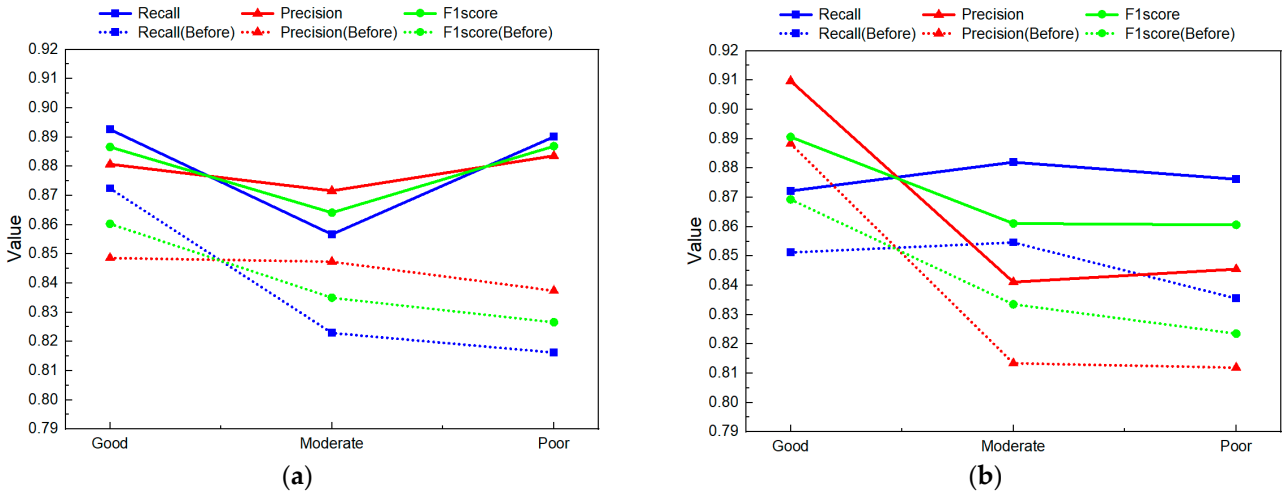


Figure 16. Comparison of model performance before and after improvement: (**a**) Prediction of cement bond quality at the casing–cement sheath interface; (**b**) Prediction of cement bond quality at the cement sheath–formation interface.

5. Field Test

To evaluate the applicability and predictive capability of the proposed model under real-field conditions, this study utilizes cementing operation data and corresponding acoustic amplitude logging results from the third-stage casing section of a well in the Tarim Oilfield to conduct a cement bond quality prediction. The well parameters are as follows: the borehole diameter is 311.2 mm, and a conventional cementing process was employed. The cementing depth reaches 5537 m, with a drilling fluid density of 1.92 g/cm^3, and the cement slurry was returned to the surface. The second-stage casing was set at a depth of 3708 m, resulting in a dual-casing section from 0 to 3708 m and a single-casing section from 3708 to 5298 m. This study focuses exclusively on the cement bond quality evaluation and modeling of the single-casing interval (3708–5298 m). The cement slurry was prepared with a water-to-cement ratio of 0.35. During the operation, the slurry exhibited an average density of 1.93 g/cm^3, with an average displacement rate of 42 L/s and a pump pressure of approximately 10 MPa. The rheological properties of the cement slurry were measured on-site using a rotational viscometer. Detailed parameters are provided in Appendix B.

By inputting the field data from this well into the trained cement bond quality prediction model, the predicted results for each meter of the cemented interval were obtained, as

shown in Figure 17. Subsequently, a comparison was made between the predicted results and the acoustic amplitude evaluation outcomes, and a confusion matrix was constructed, as shown in Figure 18, to visualize the classification performance of the model.

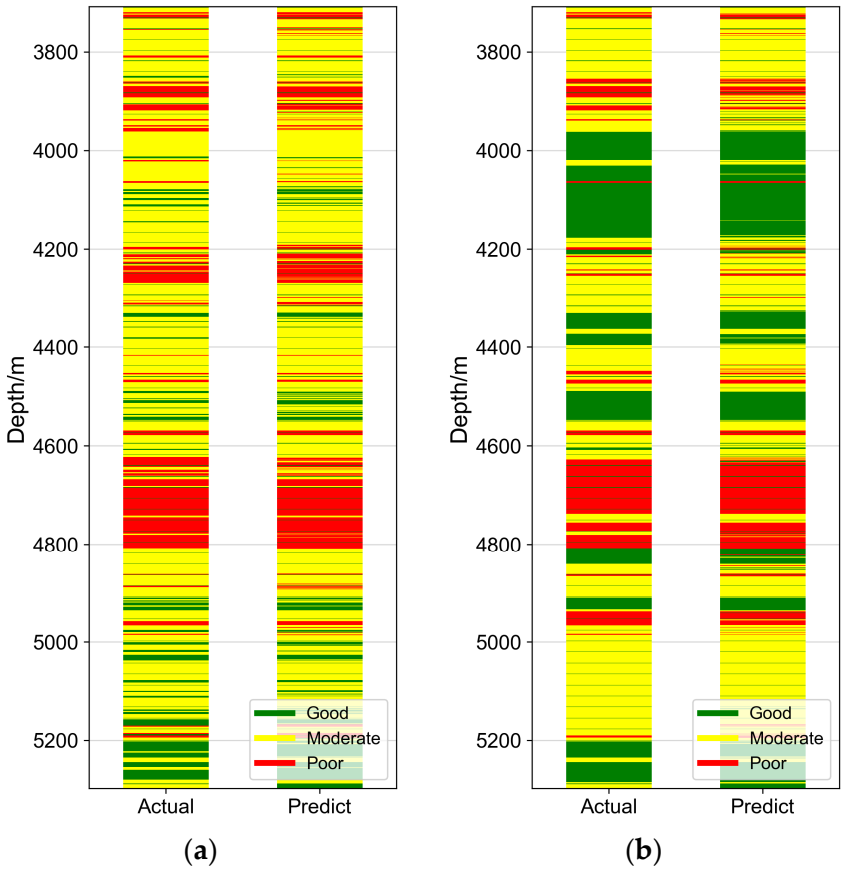


Figure 17. Cement bond quality prediction results for the 3708–5298 m interval: (**a**) Casing–cement sheath interface. (**b**) Cement sheath–formation interface.

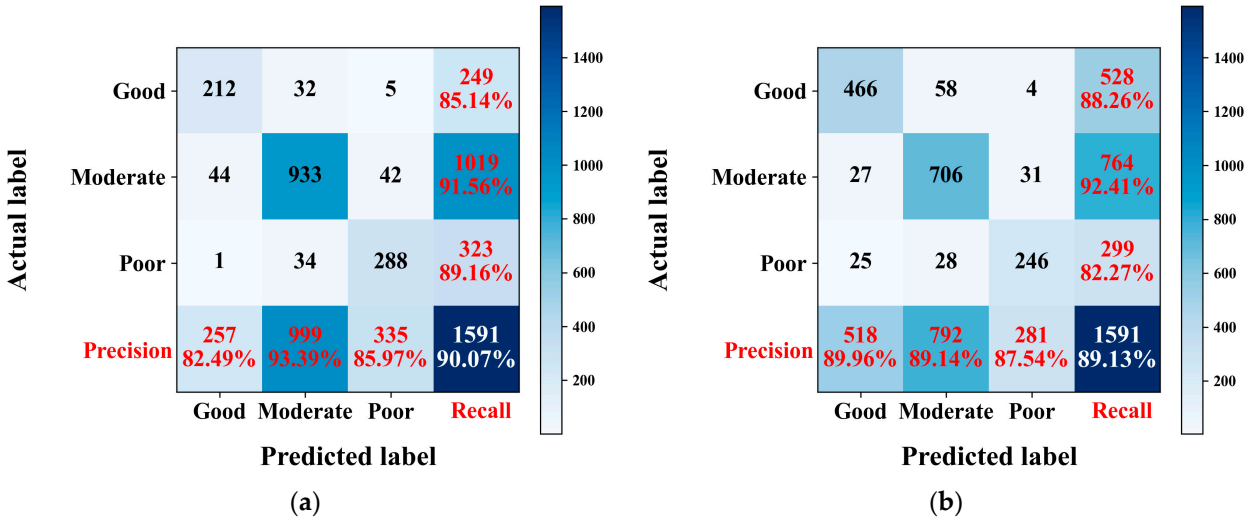


Figure 18. Confusion matrices of the field test results: (**a**) cement bond quality at the casing–cement sheath and (**b**) cement bond quality at the cement sheath–formation interface.

As shown in Figure 18, the proposed model achieves a prediction accuracy of 90% for the cement sheath quality at the casing interface and 89% at the second interface. These

results indicate that the model is capable of accurately predicting cementing quality at both interfaces, demonstrating strong potential for practical field applications.

6. Discussion

This section discusses the advantages, limitations, and future development directions of the model.

Advantages:

High Prediction Accuracy: This method integrates the cement slurry rheological equation into the Wide and Deep neural network framework, further improving prediction accuracy compared with traditional neural network methods and enhancing the model's capability to recognize cement bond quality.

Good Generalization Ability: The model has demonstrated stable performance on the test dataset, indicating strong generalization ability and maintaining high accuracy across different data distributions.

Limitations:

Dependence on Data Quality: The model's performance heavily relies on the quality and diversity of the training data. If there is bias in data collection, the prediction capability may be affected, leading to reduced generalization in certain complex conditions.

Applicability of Azimuthal Factors: Correlation analysis in this study indicates that azimuth has little impact on the model. This assumption is reasonable when the influence of the formation's horizontal stress direction is insignificant. However, in tectonically active basins, azimuth may play a crucial role in wellbore stability, and its effect may need to be further considered in specific application scenarios.

Influence of Formation Pressure: Formation pressure also affects cementing quality. The formations considered in this study are all normally compacted formations, without abnormally high or low pressure zones. As a result, pressure data were excluded from the correlation analysis, and only well depth was retained. However, in abnormally compacted formations, this factor must be considered. Additionally, the rheological properties of cement slurry are also affected by pressure. However, current field tests of cement slurry rheology in oilfields are typically conducted under atmospheric pressure, meaning that no high-pressure experimental data are available for modifying the power-law model. This limitation may impact prediction results.

Future Development Directions:

Future research will focus on integrating laboratory-based cement slurry testing with intelligent modeling to more accurately simulate downhole conditions. Although the current model incorporates several key influencing factors, there remains considerable room for enhancement. For instance, plastic contraction of the cement slurry, which can significantly impact the integrity of the cement sheath, should be considered in subsequent studies. Additionally, other cement slurry properties—such as thickening time—could also be incorporated. These properties can be quantified through laboratory tests conducted prior to field operations and subsequently used as model inputs, thereby enabling a more precise characterization of cement slurry behavior under downhole conditions.

7. Conclusions

This study proposes an improved cement bond quality prediction method based on the Wide and Deep neural network. By incorporating the rheological characteristics of cement slurry and embedding the temperature-corrected equations for the consistency coefficient and flow behavior index into the network structure, the model can more accurately characterize the flow behavior of cement slurry under varying temperature

and shear conditions, thereby significantly enhancing the prediction accuracy of cement bond quality.

Experimental results show that the optimized Wide and Deep model outperforms traditional neural network models in terms of recall, precision, and F1-score. The overall accuracy reaches 87%, representing an improvement of approximately 4%, with a particularly notable enhancement of 6% in identifying Poor (low-quality bond) cases. Furthermore, the model was validated using real field data from the third-stage cementing section of an actual well. The predicted results were compared with acoustic amplitude logging evaluations, achieving a prediction accuracy of 89%, thus demonstrating excellent field applicability.

To further investigate the impact of physical knowledge embedding on model training, two models with identical architectures were designed: one with embedded physical equations and the other using traditional weight-based computations. Gradient analysis during training revealed that the conventional model was prone to gradient vanishing, whereas the model with embedded physical equations achieved stable convergence while maintaining nonzero gradients. This ensured continuous weight updates and improved prediction accuracy. These findings explain, from a gradient perspective, how embedding physical knowledge enhances model performance.

The Wide and Deep intelligent prediction approach proposed in this study provides an efficient and accurate decision-support tool for cement bond quality evaluation. It can also be applied to optimize cementing parameters and reduce operational risks, offering both theoretical foundation and practical guidance for the advancement of intelligent cementing technologies.

Author Contributions: Conceptualization, R.L. and J.Y.; methodology, J.Y.; software, L.L.; validation, L.L.; writing—review and editing, Z.W.; formal analysis, Z.W.; investigation, S.Z.; investigation, S.Z.; data curation, S.Z.; resources, Z.Z.; data curation, Z.Z.; writing—original draft preparation, R.L.; writing—review and editing, R.L.; visualization, R.L.; supervision, R.L.; project administration, J.Y.; funding acquisition, R.L. All authors have read and agreed to the published version of the manuscript.

Funding: This research was funded by the Joint Funds of the National Natural Science Foundation of China (Grant No. U22B6003).

Institutional Review Board Statement: This study does not involve humans or animals. Therefore, the Institutional Review Board Statement is not applicable.

Informed Consent Statement: This study does not involve human participants. Therefore, the informed consent statement is not applicable.

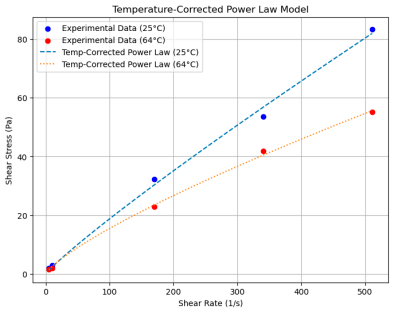
Data Availability Statement: The authors do not have permission to share data.

Conflicts of Interest: Author Rengguang Liu, Luo Liu and Shiming Zhou were employed by the company SINOPEC Research Institute of Petroleum Engineering Co., Ltd. The remaining authors declare that the research was conducted in the absence of any commercial or financial relationships that could be construed as a potential conflict of interest.

Appendix A

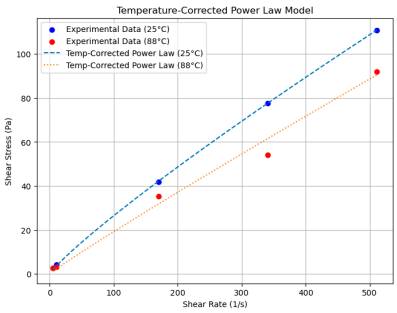
The rheological calculation results of cement slurry for the remaining wells in this study are shown in the figures.

From Figure A1, it can be seen that the cement slurry applied in this study conforms to the power-law model. Moreover, the fitting performance of the model improves after temperature correction.



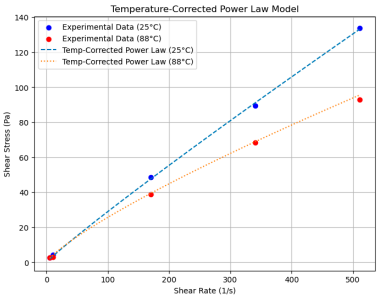
$k_0 = 0.294473$, $C_k = -0.005220$, $n_0 = 0.902377$,
$C_n = 0.002065$, $R^2 = 0.997430$

(**a**)



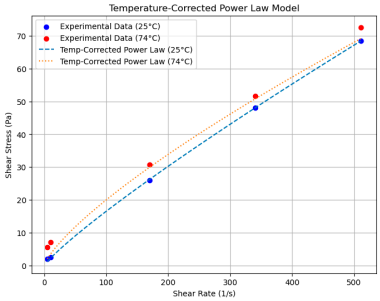
$k_0 = 0.462506$, $C_k = 0.010349$, $n_0 = 0.87860$,
$C_n = -0.001250$, $R^2 = 0.995361$

(**b**)



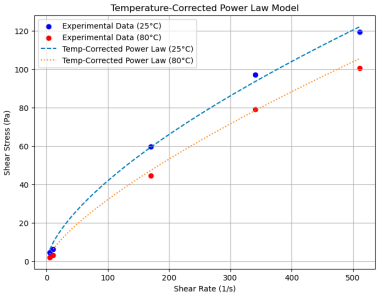
$k_0 = 0.391048$, $C_k = -0.007518$, $n_0 = 0.934853$,
$C_n = 0.002360$, $R^2 = 0.999629$

(**c**)



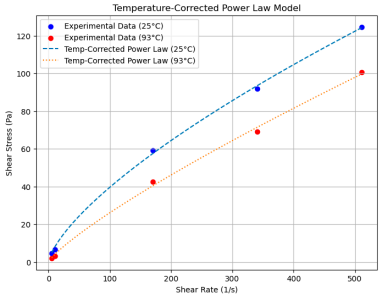
$k_0 = 0.300670$, $C_k = -0.014201$, $n_0 = 0.870246$,
$C_n = 0.002755$, $R^2 = 0.996245$

(**d**)



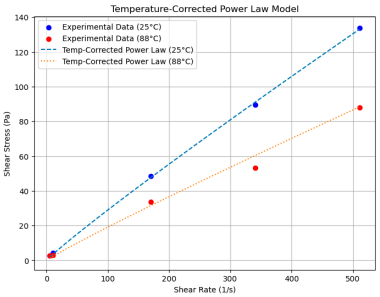
$k_0 = 2.044751$, $C_k = 0.011044$, $n_0 = 0.655799$,
$C_n = -0.001944$, $R^2 = 0.997132$

(**e**)



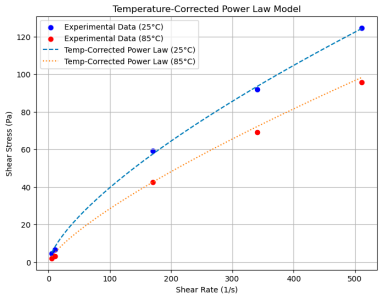
$k_0 = 1.575183$, $C_k = 0.014335$, $n_0 = 0.700386$,
$C_n = -0.002343$, $R^2 = 0.998968$

(**f**)



$k_0 = 0.391049$, $C_k = 0.006966$, $n_0 = 0.934852$,
$C_n = -0.000079$, $R^2 = 0.997242$

(**g**)



$k_0 = 1.575183$, $C_k = 0.010190$, $n_0 = 0.700386$,
$C_n = -0.001378$, $R^2 = 0.999260$

(**h**)

Figure A1. All rheological fitting curves of cement slurry in this study: (**a**) Experimental data and model fitting for Well C at 25 °C and 64 °C; (**b**) Experimental data and model fitting for Well C at 25 °C and 88 °C; (**c**) Experimental data and model fitting for Well D at 25 °C and 88 °C; (**d**) Experimental data and model fitting for Well D at 25 °C and 74 °C; (**e**) Experimental data and model fitting for Well E at 25 °C and 80 °C; (**f**) Experimental data and model fitting for Well F at 25 °C and 93 °C; (**g**) Experimental data and model fitting for Well G at 25 °C and 88 °C; (**h**) Experimental data and model fitting for Well H at 25 °C and 85 °C.

Appendix B

Table A1. The rotational viscometer readings of the cement slurry used in the third-stage field cementing operation.

Temperature	3	6	100	200	300
25 °C	6	9	87	152	236
88 °C	4	7	79	133	203

The fitting results of the consistency coefficient and flow behavior index are as follows:

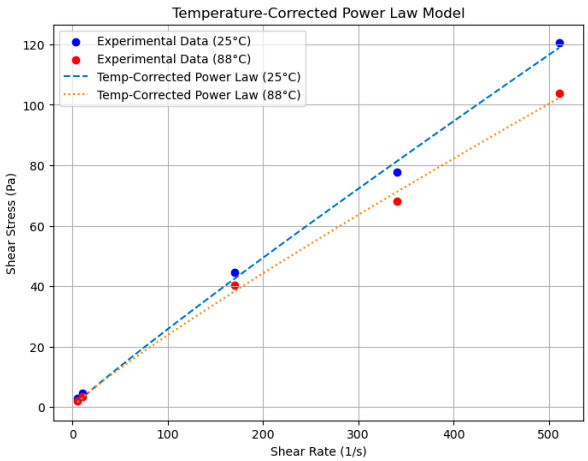


Figure A2. Fitting results of the rheological curves for the third-stage cementing slurry.

$$k_0 = 0.3468,\ C_k = -0.0019,\ n_0 = 0.9359,\ C_n = 0.0007,\ R^2 = 0.9976$$

References

1. Tang, J.; Zhang, C.G.; Zhang, B.X.; Shi, F.F. Cement bond quality evaluation based on acoustic variable density logging. *Pet. Explor. Dev.* **2016**, *43*, 514–521. [CrossRef]
2. Zhang, X.G.; Gao, X.Y.; Feng, M. Analysis of factors affecting cementing quality. *Drill. Process.* **2002**, *25*, 4. [CrossRef]
3. Xue, M.; Chu, Z.H.; Li, Y.H.; Jiang, H.; Zhao, B.C.; Chen, X.D. Discussion on several issues regarding the interpretation and evaluation of cementing quality. *Log. Technol.* **2000**, *24*, 6. [CrossRef]
4. Guo, X.Y.; Yang, Y.G.; Li, Z.Y.; Yang, X.Y. Discussion on the key factors to improve the cementing quality of complex wells. *Drill. Fluids Complet. Fluids* **2005**, *22*, 53–58. [CrossRef]
5. Li, X.; Wang, J.; Sun, T. Construction of cementing quality evaluation method system and analysis of influencing factors. *Sci. Technol. Bull.* **2017**, *33*, 68–75. [CrossRef]
6. Kinoshita, T.; Izuhara, W.; Valero, H.; Blyth, M. Feasibility and challenge of quantitative cement evaluation with LWD sonic. In Proceedings of the SPE Annual Technical Conference and Exhibition, New Orleans, LO, USA, 30 September 2013. [CrossRef]
7. Sun, Z.C. Research on the Evaluation and Statistical Analysis Technology of Cementing Quality in the Adjustment Wells of Daqing. Master's Thesis, Northeast Petroleum University, Daqing, China, 2009.
8. Ai, C.; Bu, Z.D.; Zhao, W.C.; Li, Q. The orthogonal scale wavelet network method was used to predict cementing quality. *Oil Drill. Technol.* **2008**, *6*, 56–58. [CrossRef]
9. Sun, F. Research on Cementing Quality Prediction Method. Master's Thesis, Xi'an Shiyou University, Xi'an, China, 2012.
10. Kong, C. Cementing Quality Prediction and Safety Evaluation Based on Gray Fuzzy Neural Network. Master's Thesis, China University of Petroleum (East China), Qingdao, China, 2017.
11. Guan, R.L. Prediction of cementing quality based on least squares support vector machine. *Xinjiang Oil Gas* **2018**, *14*, 5. [CrossRef]
12. Du, D.N.; Zheng, S.J.; He, Y.Z.; Zhong, W.J.; Zhang, S.H. Cementing quality prediction method based on LM optimization neural network: A case study of block X in Shunbei oilfield. *Pet. Geol. Eng.* **2021**, *35*, 123–126. [CrossRef]
13. Zhao, D.H.; Hu, L.B. Discuss machine learning methods to predict pre-operation cementing quality. *Petrochem. Technol.* **2022**, *29*, 208–210.

14. He, Y.; Zheng, Y.Z.; Wu, B.Y. Analysis and study of the influencing factors of the whole process of deep and ultra-deep cementing. *Tech. Superv. Pet. Ind.* **2023**, *39*, 1–6. [CrossRef]
15. Nyakilla, E.E.; Jun, G.; Kasimu, N.A.; Robert, E.F.; Innocent, N.; Mohamedy, T.; Shaame, M.; Ngata, M.R.; Mabeyo, P. Application of machine learning in the prediction of compressive, and shear bond strengths from the experimental data in oil well cement at 80 °C. Ensemble trees boosting approach. *Constr. Build. Mater.* **2022**, *317*, 125778. [CrossRef]
16. Fang, C.F.; Wang, Z.; Song, X.Z.; Zhao, P.Z.; Yang, D.H.; Liu, M.C. A novel cementing quality evaluation method based on convolutional neural network. *Appl. Sci.* **2022**, *12*, 10997. [CrossRef]
17. Zhang, T.J.; Wang, D.L.; Yang, L. RheologyNet: A physics-informed neural network solution to evaluate the thixotropic properties of cementitious materials. *Cem. Concr. Res.* **2023**, *168*, 107157. [CrossRef]
18. Abdollahian, A.; Wang, H.; Liu, H.; Zheng, X.M. Transfer learning for acoustic cement bond evaluation: An image classification approach using acoustic variable Density log. *Geoenergy Sci. Eng.* **2024**, *239*, 212960. [CrossRef]
19. Zhang, J.Y.; Song, W.Y.; Guo, S.L.; Bu, Y.H.; Liu, H.J.; Li, M.Z. Experimental study on the evaluation model of cementing quality for ultra-low density cement well cluster. *Chem. Technol. Fuels Oils* **2023**, *59*, 1129–1137.
20. Kianoush, P.; Mesgari, F.; Jamshidi, E.; Gomar, M.; Kadkhodaie, A.; Varkouhi, S. Investigating the effect of hole size, bottom hole temperature, and composition on cement bonding quality of exploratory wells in Iran. *Sci. Rep.* **2024**, *14*, 29653. [CrossRef]
21. Li, Y.J.; Zhang, W.D.; Wu, J.; Yang, Y.H.; Zhang, C.; Yang, H.Q. A comprehensive method for the optimization of cement slurry and to avoid air channeling in high temperature and high-pressure conditions. *Fluid Dyn. Mater. Process.* **2022**, *19*, 1237–1248. [CrossRef]
22. Li, J.; Chen, W.J.; Liu, Z.D. Study on the influencing factors of the cementing quality evaluation and the improvement measures. In Proceedings of the International Field Exploration and Development Conference 2022, Xi'an, China, 16 November 2022. [CrossRef]
23. Spearman, C. The proof and measurement of association between Two Things. *Am. J. Psychol.* **1904**, *15*, 72–101. [CrossRef]
24. Cramér, H. *Mathematical Methods of Statistics*; Princeton University Press: Princeton, NJ, USA, 1946; p. 591.
25. McCulloch, W.S.; Pitts, W. A logical calculus of the ideas immanent in nervous activity. *Bull. Math. Biol.* **1943**, *5*, 115–133. [CrossRef]
26. Cheng, H.; Koc, L.; Harmsen, J.; Shaked, T.; Chandra, T.; Aradhye, H.; Anderson, G.; Corrado, G.; Chai, W.; Ispir, M.; et al. Wide & Deep learning for recommender systems. In Proceedings of the 1st Workshop on Deep Learning for Recommender Systems, Boston, MA, USA, 15 September 2016. [CrossRef]
27. Tao, C.C.; Kutchko, B.; Rosenbaum, E.; Massoudi, M. A Review of Rheological Modeling of Cement Slurry in Oil Well Applications. *Energies* **2020**, *13*, 570. [CrossRef]
28. Wang, L.; Liu, B.H.; Guo, Y.T.; Li, J.; Yan, H.Z.; Liu, H.J.; Heng, S. Experimental investigation of the cementation and tensile properties of cement to formation interface considering surface irregularity and drilling mud residue. *J. Pet. Explor. Prod. Technol.* **2023**, *13*, 705–721. [CrossRef]
29. Tao, C.C.; Rosenbaum, E.; Kutchko, B.; Massoudi, M. *The Importance of Vane Configuration on Yield Stress Measurements of Cement Slurry*; Technical Report DOE-NETL-2020-2072; U.S. Department of Energy, National Energy Technology Laboratory: Pittsburgh, PA, USA, 2020. Available online: https://netl.doe.gov/sites/default/files/netl-file/ImportanceofVaneConfigurationonYieldStressMeasurementsofCementSlurry_04142020.pdf (accessed on 12 February 2024).
30. Liu, J.; Zhu, J.L.; Ji, X.L.; Song, X.L.; Xue, Y.L. Study on the influence of cement slurry viscosity on acoustic emission response and deformation characteristics of slurry-coal cemented body. *Constr. Build. Mater.* **2024**, *450*, 138735. [CrossRef]
31. Bingham, E.C. Fluidity and plasticity. In *Fluidity and Plasticity*; McGraw-Hill: New York, NY, USA, 1922.
32. Newman, M. Power laws, Pareto distributions and Zipf's law. *Contemp. Phys.* **2005**, *46*, 323–351. [CrossRef]
33. Zhao, X.Y.; Luo, H.; Yang, M.; Lu, P.Q.; Zheng, Y.Z.; Li, H.T. Novel method for optimization cement slurry based on the wellbore integrity model in high-temperature and high-pressure conditions. *ACS Omega* **2023**, *8*, 45668–45677. [CrossRef]
34. Grasinger, M.; Li, Z.C.; Vuotto, A.; Brigham, J.; Lannacchione, A.; Vandenbossche, J. Simulation of cement slurry flow to assess the potential for voids and channels in wellbore cementing processes. In Proceedings of the SPE Eastern Regional Meeting, Morgantown, WV, USA, 13 October 2015. [CrossRef]

Disclaimer/Publisher's Note: The statements, opinions and data contained in all publications are solely those of the individual author(s) and contributor(s) and not of MDPI and/or the editor(s). MDPI and/or the editor(s) disclaim responsibility for any injury to people or property resulting from any ideas, methods, instructions or products referred to in the content.